


Cite this: *Chem. Sci.*, 2024, 15, 8913

All publication charges for this article have been paid for by the Royal Society of Chemistry

# High-order layered self-assembled multicavity metal–organic capsules and anti-cooperative host–multi-guest chemistry†

Kaixiu Li,<sup>a</sup> Zhengguang Li,<sup>a</sup> Jie Yuan,<sup>c</sup> Mingzhao Chen,<sup>b</sup> He Zhao,<sup>a</sup> Zhiyuan Jiang,<sup>a</sup> Jun Wang,<sup>b</sup> Zhilong Jiang,<sup>b</sup> Yiming Li,<sup>a</sup> Yi-Tsu Chan,<sup>b</sup> Pingshan Wang<sup>b</sup> and Die Liu<sup>b</sup>  <sup>\*,a</sup>

The construction and application of metal–organic cages with accessible internal cavities have witnessed rapid development, however, the precise synthesis of complex metal–organic capsules with multiple cavities and achievement of multi-guest encapsulation, and further in-depth comprehension of host–multi-guest recognition remain a great challenge. Just like building LEGO blocks, herein, we have constructed a series of high-order layered metal–organic architectures of generation  $n$  ( $n = 1/2/3/4$  is also the number of cavities) by multi-component coordination-driven self-assembly using porphyrin-containing tetrapodal ligands (like plates), multiple parallel-podal ligands (like clamps) and metal ions (like nodes). Importantly, these high-order assembled structures possessed different numbers of rigid and separate cavities formed by overlapped porphyrin planes with specific gaps. The host–guest experiments and convincing characterization proved that these capsules **G2–G4** could serve as host structures to achieve multi-guest recognition and unprecedentedly encapsulate up to four  $C_{60}$  molecules. More interestingly, these capsules revealed negative cooperation behavior in the process of multi-guest recognition, which provides a new platform to further study complicated host–multi-guest interaction in the field of supramolecular chemistry.

Received 20th February 2024  
Accepted 7th May 2024

DOI: 10.1039/d4sc01204f

[rsc.li/chemical-science](https://rsc.li/chemical-science)

## Introduction

The pursuit of mimicking the structure and functionality of biological systems has prompted chemists to synthesize more elegant and complicated supramolecular assemblies.<sup>1</sup> In this process, coordination-driven supramolecular assembly has become the preferred strategy due to its self-organization and predictability.<sup>2–5</sup> A very diverse library of supramolecular architectures with well-defined shapes and sizes has been created, and pioneering contributions include metallo-macrocycles,<sup>6–8</sup> platonic polyhedra,<sup>9–11</sup> metal–organic cages,<sup>12–14</sup> intricate molecule knots<sup>15–17</sup> and so on.<sup>18–20</sup> Highly sophisticated structures, such as the DNA double helix and virus capsid structure, can be

constructed *via* supramolecular self-assembly in nature. However, the level of size and complexity of most artificial metal–organic supramolecular architectures employed to date lags far behind that of nature. Although remaining a formidable challenge, there are still creative efforts focused on developing construction strategies of complicated metal–organic supramolecules, such as low-symmetry metal–organic cages,<sup>19–21</sup> interlocked molecular assemblies,<sup>22–25</sup> giant metal-based supramolecules<sup>13,26</sup> and so on.<sup>7,27</sup>

To achieve structural complexity and further diverse functionalities, the coordination-driven supramolecular cages may be the most suitable candidate due to the significant cavity, which can be exploited in diverse fields, such as biomedicine,<sup>28</sup> separation,<sup>29</sup> catalysis,<sup>30,31</sup> and so on.<sup>32</sup> However, most of the efforts have been focused on the metal–organic polyhedron featuring one single cavity.<sup>33,34</sup> Therefore, the construction methods of metal–organic capsules with multiple cavities, namely multiple separate cavities in a single entity, are highly desirable.<sup>35,36</sup> Three strategies are available to create multiple cavities in metallo-supramolecular architectures: interpenetrating architectures to increase the number of cavities,<sup>37–39</sup> vertical extension of single cavity systems<sup>40–45</sup> and expanding the structure on a two-dimensional plane.<sup>46,47</sup> For example, Crowley *et al.* reported the first example of a  $[Pd_4(L)_4]^{8+}$  cage with three cavities using the long backboned multi-pyridine ligands.<sup>43</sup>

<sup>a</sup>Department of Organic and Polymer Chemistry, Hunan Key Laboratory of Micro & Nano Materials Interface Science, College of Chemistry and Chemical Engineering, Central South University, Changsha, Hunan-410083, China

<sup>b</sup>Department Institute of Environmental Research at Greater Bay Area, Key Laboratory for Water Quality and Conservation of the Pearl River Delta, Ministry of Education, Guangzhou Key Laboratory for Clean Energy and Materials, Guangzhou University, Guangzhou-510006, China

<sup>c</sup>School of Chemistry and Chemical Engineering, Henan Normal University, Xinxiang, Henan 453007, China

<sup>d</sup>Department of Chemistry, National Taiwan University, Taipei 10617, Taiwan

† Electronic supplementary information (ESI) available. See DOI: <https://doi.org/10.1039/d4sc01204f>

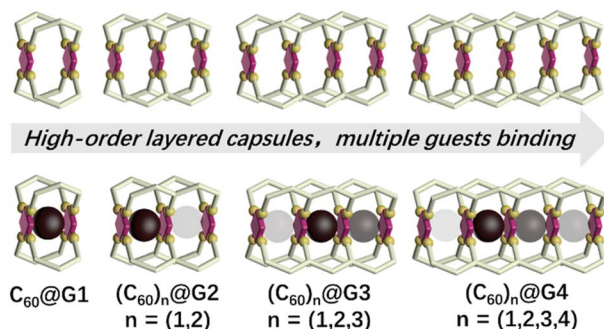


Fig. 1 Cartoon representation of a series of multi-cavity cages and their  $C_{60}$  complexes (the darker colored ball represents a more prioritized binding).

Soon after, Clever's group synthesized a peanut-shaped cage by assembling a tris-monodentate ligand with  $Pd^{II}$  cations, followed by quantitative catenation to give a five-cavity-containing compound.<sup>37</sup> However, the previously reported multi-cavity supramolecular capsules can only recognize multiple anions or small molecules due to a small cavity volume.<sup>43–45</sup> By comparison, those capsules being able to encapsulate large guests have rarely been documented due to the difficulties in synthesis and the assembly strategy.<sup>42</sup> Moreover, the reports of cooperative behaviors of the homotropic binding or heterotropic binding guests in multi-cavity capsules remain elusive in spite of the fact that such behavior has been intensively investigated in a single cavity.<sup>36</sup> Therefore, constructing capsules with multiple large cavities and further researching the mutual influence between the host and binding large guests is meaningful, yet especially challenging.

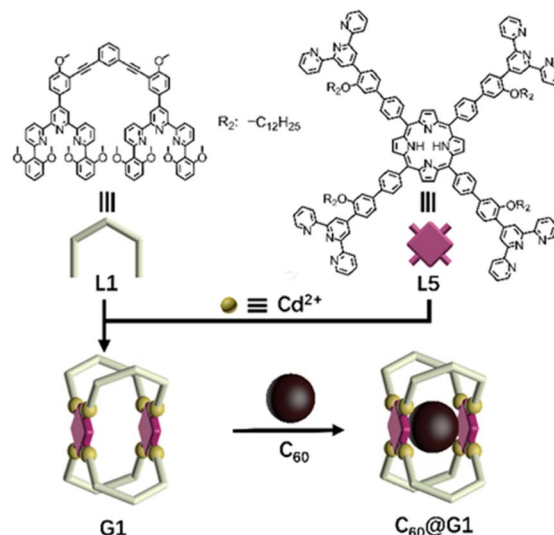
Encouraged by previous excellent and appealing studies on multi-cavity cages, herein, a series of layered metal-organic capsules with large cavities varying from one to four pockets have been synthesized *via* the multicomponent self-assembly of terpyridine ligands and  $Cd^{2+}$ . Furthermore, the large guest fullerene ( $C_{60}$ ) can be homogeneously bound by these capsules. Particularly noteworthy are the discrete single-molecular capsules that can wrap up to four  $C_{60}$  molecules (Fig. 1). More interestingly, based on the results of experimental and theoretical calculations, the negative cooperation effect between binding  $C_{60}$  has been also revealed.

## Results and discussion

### Assembly and characterization of metal-organic capsule G1

Initially, as shown in Scheme 1, G1 with one cavity was designed. In order to avoid the self-sorting and realize the heteronuclear recognition in the process of coordination-driven assembly,<sup>48</sup> L1 modified with 2,6-dimethoxyphenyl as a steric hindrance group at the 6,6'' position and L5 were obtained by Sonogashira and Suzuki coupling reactions, respectively, which were characterized using the  $^1H$  NMR, 2D COSY, 2D NOESY and ESI-MS spectra (Fig. 2A, S21–S24, S43–S46, S53 and S57†).

The assembly of G1 was carried out by mixing L1, L5 and  $Cd(NO_3)_2 \cdot 4H_2O$  at a precise stoichiometric ratio of 2 : 1 : 4 in



Scheme 1 Chemical structure of ligands L1 and L5, and schematic illustration of the self-assembly and host-guest recognition to  $C_{60}$  of G1.

MeOH/ $CHCl_3$  (1 : 1) and heating at 70 °C for 8 h (Scheme 1). After cooling to room temperature, an excessive  $CH_3OH$  solution of  $NH_4PF_6$  was added to exchange the anion  $NO_3^-$  to  $PF_6^-$ ,

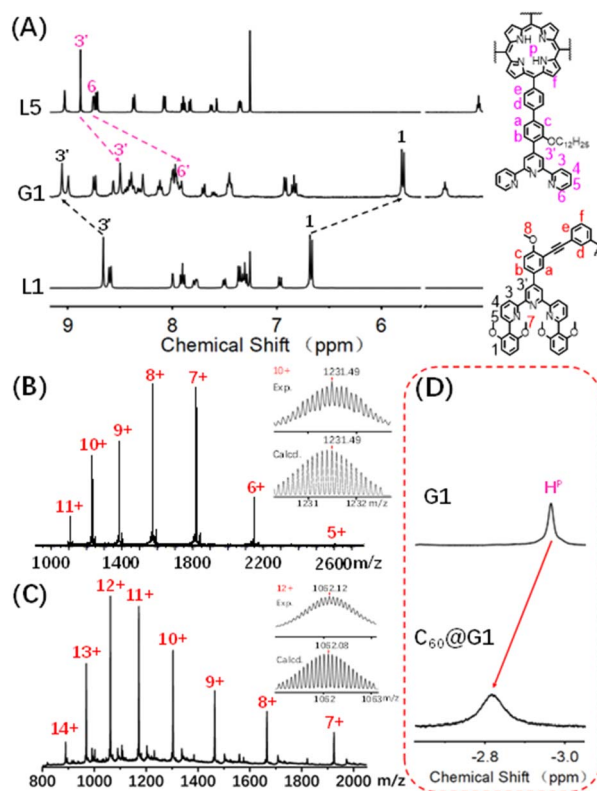


Fig. 2 (A)  $^1H$  NMR spectra (500 MHz, 298 K) of supramolecule G1 in  $CD_3CN$  and L1 and L5 in  $CDCl_3$ ; ESI-MS spectra of the (B) G1 and (C)  $C_{60}@G1$  (inset: isotopic distribution patterns); (D) partial  $^1H$  NMR spectra (600 MHz, 298 K) of G1 to highlight the shift of the proton  $H^P$ .

giving a deep purple precipitate. Based on the comparison of  $^1\text{H}$  NMR spectra of **L1**, **L5** and supramolecular **G1**, the  $\text{tpy-H}^{3'}$  of ligand **L1** shifted to the low-field ( $\delta = 9.09$  ppm,  $\Delta\delta = 0.43$  ppm) due to the electron-withdrawing effect of the metal center after coordination with  $\text{Cd}^{2+}$ . In contrast, the  $\text{tpy-H}^{3'}$  of ligand **L5** shifted to high-field ( $\delta = 8.53$  ppm,  $\Delta\delta = 0.37$  ppm) in **G1** because of the strong shielding effect of 2,6-dimethoxyphenyl groups. These results indicated that **L1** and **L5** had formed heteronuclear coordination assembly (Fig. 2A). Moreover, two characteristic signals of  $\text{tpy-H}^{3'}$  displayed an integral ratio of 1 : 1, and the triple peak at 4.63 ppm combining with two singlet peaks at 4.17 and 2.77 ppm in the non-aromatic region, respectively attributed to the methylene and methoxyl groups, showed an integral ratio of 2 : 3 : 12, which was completely consistent with the desired structure (Fig. S62 and S63†). All proton signals were fully assigned by 2D COSY and 2D NOESY, verifying the successful formation of **G1** (Fig. S64 and S65†). Through ESI-MS, a series of signal peaks from +11 to +5 corresponding to moieties of continuously losing various numbers of  $\text{PF}_6^-$  were observed. And the experimental charge-to-mass ratio ( $m/z$ ) values were consistent with the calculated ones (Fig. 2B and S80†). Further, TWIM-MS presented a group of signals ranging from +11 to +6, with a narrow drift time and no signal of other isomers, indicating that a single and discrete species **G1** was formed (Fig. S79†).

### Host-guest interaction of **G1** and $\text{C}_{60}$

Based on previous reports, the porphyrin-containing cages were able to encapsulate large aromatic molecules,<sup>49</sup> such as fullerene,<sup>46,50–52</sup> via suitable internal cavities and strong  $\pi$ - $\pi$  interaction. With this in mind, the host-guest recognition of **G1** was performed with  $\text{C}_{60}$  as the guest molecule in which the  $\text{C}_{60}$  solid (**G1** :  $\text{C}_{60}$  molar ratio 1 : 3) was added to 0.6 mL (10.0 mg  $\text{mL}^{-1}$ )  $\text{CD}_3\text{CN}$  solution of capsule **G1**, and further heated at 80 °C for 24 hours. As shown in Fig. 2D and S94,† the characteristic signal of pyrrole protons ( $\text{H}^{\text{P}}$ ) in porphyrin rings was observed as one single peak and shifted from  $-2.93$  ppm to low-field ( $-2.79$  ppm) after the addition of  $\text{C}_{60}$ , demonstrating that  $\text{C}_{60}$  was enveloped inside the cavity rather than on the periphery of **G1**.<sup>53</sup> In order to further support the conclusion, the single-layered complex **G0** was synthesized (Fig. S58–S61†). The  $^1\text{H}$  NMR signals of **G0** clearly showed no change after mixing with  $\text{C}_{60}$  under the same conditions, manifesting that there was no obvious binding between single-layered porphyrin and  $\text{C}_{60}$  (Fig. S91†). Such results also excluded the possibility that  $\text{C}_{60}$  molecules were sitting outside each cavity and interacted with the external faces of the porphyrin walls in **G1**. Additionally, comparing the  $^{13}\text{C}$  NMR of  $\text{C}_{60}$ @**G1** with **G1** in  $\text{CD}_3\text{CN}$ , a sharp single peak at 140.4 ppm appeared and can be assigned to encapsulated  $\text{C}_{60}$ , supported by the fact that the  $^{13}\text{C}$  NMR signal of the sole  $\text{C}_{60}$  cannot be collected due to the negligible solubility in  $\text{CD}_3\text{CN}$  (Fig. S95†). Further, the ESI-MS displayed a set of charged peaks from +14 to +7, which perfectly matched with  $\text{C}_{60}$ @**G1** instead of  $(\text{C}_{60})_2$ @**G1** or empty **G1** (Fig. 2C and S96†). But for the mixture of **G0** and  $\text{C}_{60}$ , no ESI-MS signals attributed to  $(\text{C}_{60})_n$ @**G0** were observed (Fig. S92†). All these pieces of

evidence proved that one  $\text{C}_{60}$  was located in the cavity of **G1**. Next, rigorous measurements of the binding constant were conducted by UV-vis titration of **G1** with  $\text{C}_{60}$  solution in DMF. The formation of the  $\text{C}_{60}$ @**G1** complex was characterized by a substantial decrease of band intensity at 442 nm and a successive increase at 425 nm in comparison with that of **G1** itself (Fig. S118†). Further, the binding constant was calculated to be  $(2.9 \pm 0.6) \times 10^4 \text{ M}^{-1}$  in DMF on the basis of a 1 : 1 binding mode<sup>54</sup> (Fig. S117–S119†). The kinetic process of **G1** wrapping  $\text{C}_{60}$  was investigated through time-dependent  $^1\text{H}$  NMR experiments, in which the time to reach equilibrium state at 333 K and 353 K was determined to be approximately 17 h and 13 h, respectively. Then the activation energy ( $E_a$ ) to encapsulate  $\text{C}_{60}$  for **G1** was calculated to be  $35.32 \text{ kJ mol}^{-1}$  according to the Arrhenius formula (Fig. S120–S123†). Finally, the total energies ( $E$ ) of **G1**,  $\text{C}_{60}$ @**G1**, and  $\text{C}_{60}$  were calculated by the semiempirical quantum mechanical GFN1-xTB method,<sup>55</sup> resulting in  $\Delta E = -23.47 \text{ kcal mol}^{-1}$  from discrete **G1** and  $\text{C}_{60}$  to complex  $\text{C}_{60}$ @**G1** (Fig. S127†). These results demonstrated that **G1** had strong binding affinities, yet high activation energy to  $\text{C}_{60}$ . The above-mentioned performances indicated that cage **G1** possessed the suitable cavities and was a perfect host to encapsulate  $\text{C}_{60}$ .

### Assembly and characterization of metal-organic capsules **G2**–**G4**

The successful assembly and host-guest interaction of **G1** proved that the heteronuclear assembly strategy was feasible to construct host capsules. Therefore, the work returned to the original idea to obtain multi-cavity supramolecules by similar construction methods. Multilevel ligands **L2**–**L4** were obtained by Sonogashira coupling reactions, respectively, which were characterized using the  $^1\text{H}$  NMR, 2D COSY, 2D NOESY and ESI-MS spectra (Fig. S25–S38, S54 and S56†).

By using a similar method to **G1**, multi-cavity supramolecular capsules **G2**–**G4** were obtained by heating the mixture of ligands **L2**/**L3**/**L4**, **L5** and  $\text{Cd}(\text{NO}_3)_2 \cdot 4\text{H}_2\text{O}$  at accurate stoichiometric ratios (Fig. 3). The structural evidence of supramolecular **G2**–**G4** was first collected by NMR experiments. Despite the large size and complicated composition of assembled architectures, sharp and distinct  $^1\text{H}$  NMR patterns were still obtained. From the comparison of **G2**–**G4** with corresponding ligands (**L2**–**L5**), the signals assigned to the  $\text{tpy-H}^{3'}$  situated on ligands **L2**/**L3**/**L4** showed low-field upon complexation, whereas the  $\text{tpy-H}^{3'}$  and the  $\text{tpy-H}^6$  located at ligand **L5** obviously shifted to high-field due to the shielding effect of 2,6-dimethoxyphenyl, respectively, supporting the formation of complexes (Fig. 4A, S82 and S85†). Further exemplified with **G3**, as shown in Fig. 4A, structural information was collected: (i) four characteristic single peaks at 9.11, 9.03, 8.42 and 8.35 ppm attributed to  $\text{tpy-H}^{3'}$  with an integral ratio of 1 : 1 : 1 : 1 were observed; (ii) three triple peaks at 4.70 ppm, 4.52 ppm, and 4.34 ppm showed an integral ratio of 1 : 2 : 1 attributed to  $-\text{OCH}_2-$ , and two single peaks at 2.68 and 2.51 ppm with an integral ratio of 1 : 1 attributed to  $-\text{OCH}_3$ ; (iii) two single peaks at  $-3.03$  and  $-3.32$  ppm with an integral ratio of 1 : 1 attributed to pyrrole proton  $\text{H}^{\text{P}}$  (Fig. S70 and S71†). The integral ratio of these





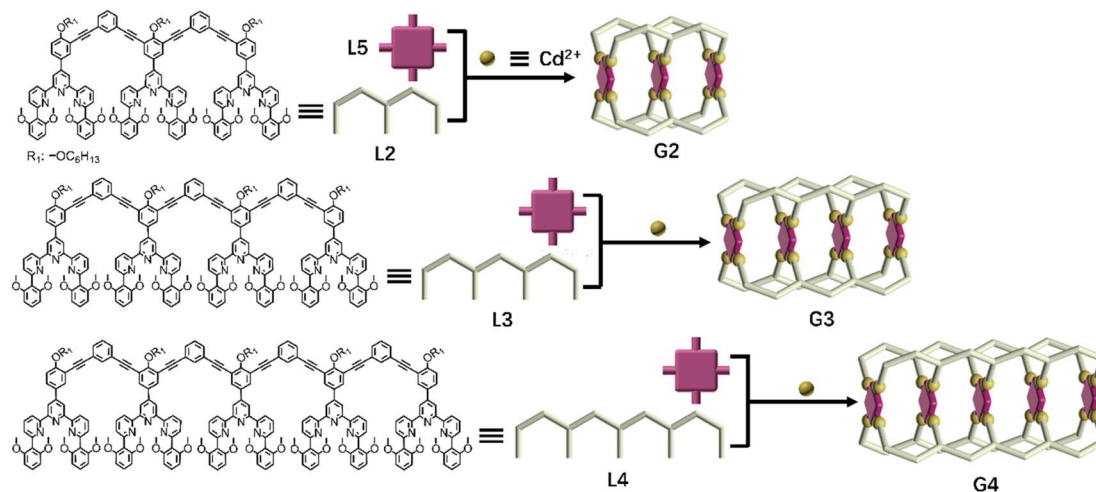


Fig. 3 Chemical structure of ligands L2–L4 and schematic illustration of multicomponent self-assembly of multideck complex metal–organic capsules G2–G4.

characteristic peaks was completely consistent with the desired structure. Similarly, the detailed structural analysis of G2 and G4 was also presented in the ESI.† The attribution of all protons through the  $^1\text{H}$  NMR, 2D COSY and NOESY proved the successful assembly of the supramolecular cages G2–G4 (Fig. S66–S77†).

ESI-MS and TWIM-MS experiments were also performed to confirm the composition of G2–G4. A series of peaks with continuous mass charge ratio ( $m/z$ ) from +16 to +7, +22 to +10 and +22 to +12 respectively correspond to charged moieties of G2  $\{[\text{Cd}_{12}\text{L}_2\text{L}_3(\text{PF}_6^-)_{24}]n\text{PF}_6^-\}^{n+}$  ( $n = 7-16$ ) (Fig. S83A†), G3  $\{[\text{Cd}_{16}\text{L}_3\text{L}_4(\text{PF}_6^-)_{32}]n\text{PF}_6^-\}^{n+}$  ( $n = 10-22$ ) (Fig. 4B) and G4  $\{[\text{Cd}_{20}\text{L}_4\text{L}_5(\text{PF}_6^-)_{40}]n\text{PF}_6^-\}^{n+}$  ( $n = 12-22$ ) (Fig. S86A†). Further investigation revealed that the experimental  $m/z$  values matched well with theoretical values of G2 (with a molecular weight of 21 731.48 Da), G3 (with a molecular weight of 29 138.14 Da) and G4 (with a molecular weight of 36 544.80 Da), respectively. In addition, TWIM-MS spectra showed a series of bands with a narrowly distributed drifting time at each charge state from +16 to +7 (Fig. S83B†), +18 to +9 (Fig. 4C) and +21 to +16 (Fig. S86B†) for G2–G4, respectively. And no signals of other unexpected isomers were found, verifying accurate assembly of single and discrete species.

## 2D DOSY, TEM, and AFM characterization of G1–G4

Although many efforts have been devoted to cultivating single crystals, and even the crystals of G1 and  $\text{C}_{60}\text{@G1}$  were formed (Fig. S81†), unfortunately, no resolvable datum was obtained essentially due to large sizes and cavities with a large amount of unordered solvent molecules. In order to obtain more structural evidence of G1–G4, 2D DOSY, AFM and TEM characterization experiments were performed. The single band in the DOSY spectrum of G1–G4 confirmed that only one species was present in the solution. Furthermore, the diffusion coefficients from G1 to G4 increased sequentially, with  $\log D = -9.70, -9.75, -9.77$  and  $-9.91 \text{ m}^2 \text{ s}^{-1}$ , respectively (Fig. S87†). Subsequently, by calculating using the Stokes–Einstein equation, the

experimental hydrodynamic radius was 3.0, 3.3, 3.5 and 4.8 nm, respectively, which matched the sizes of the molecular modeling structure (Fig. S88†). In addition, AFM experiments were carried out by spin-coating  $\text{CH}_3\text{CN}$  solutions of G1–G4 (concentration of  $\sim 10^{-7} \text{ M}$ ) onto the freshly cleaved mica surface and showed average vertical heights of 1.5 nm (Fig. 5A, E and I), 2.6 nm (Fig. 5B, F and J), 3.7 nm (Fig. 5C, G and K), and 4.8 nm (Fig. 5D, H and L), which is well consistent with the heights in molecular modelling, respectively. The measured width of these molecules from AFM profiles showed a large value because of the tip broadening effect.<sup>56,57</sup> Meanwhile, the TEM images showed the dispersion of individual spots with average sizes fitting with the molecular models (Fig. S90†).

## Host–guest interaction of G2–G4 and $\text{C}_{60}$

Coupled with the above-mentioned host G1 being able to encapsulate  $\text{C}_{60}$  molecules, the successful synthesis of complicated multi-layered structures G2–G4 with various numbers of cavities make it feasible to research multi-guest recognition interactions, which have seldom been reported due to the synthetic obstacle.<sup>42,58,59</sup> Hence, multiple  $\text{C}_{60}$  wrapping experiments were conducted, in which  $\text{C}_{60}$  solid [ $n$  (cavity):  $n$  ( $\text{C}_{60}$ ) = 1 : 3] was added to 0.6 mL  $10.0 \text{ mg mL}^{-1}$   $\text{CD}_3\text{CN}$  solution of capsules G2–G4, respectively. And further heating at  $80^\circ\text{C}$  for 24 hours was performed to reach the thermodynamic equilibrium state, which was verified by the unchangeable  $^1\text{H}$  NMR signals (Fig. S101, S108 and S114†). Comparison of the  $^1\text{H}$  NMR spectra of G2–G4 in  $\text{CD}_3\text{CN}$  before and after adding  $\text{C}_{60}$  molecules showed that the resonance signals of characteristic pyrrole  $\text{H}^{\text{P}}$  had obvious shifts, verifying the  $\text{C}_{60}$  encapsulation. However, complex multiple sets of peaks were present owing to the complex chemical environment of  $\text{H}^{\text{P}}$  after accommodating different numbers of  $\text{C}_{60}$  molecules in the cage cavities (Fig. 6B, E, G, S98, S106 and S112†).

In terms of host capsule G2, the host–guest recognition complex system  $(\text{C}_{60})_n\text{@G2}$  consisted of three species, namely G2,  $\text{C}_{60}\text{@G2}$  and  $(\text{C}_{60})_2\text{@G2}$ , which was proved by NMR and ESI-



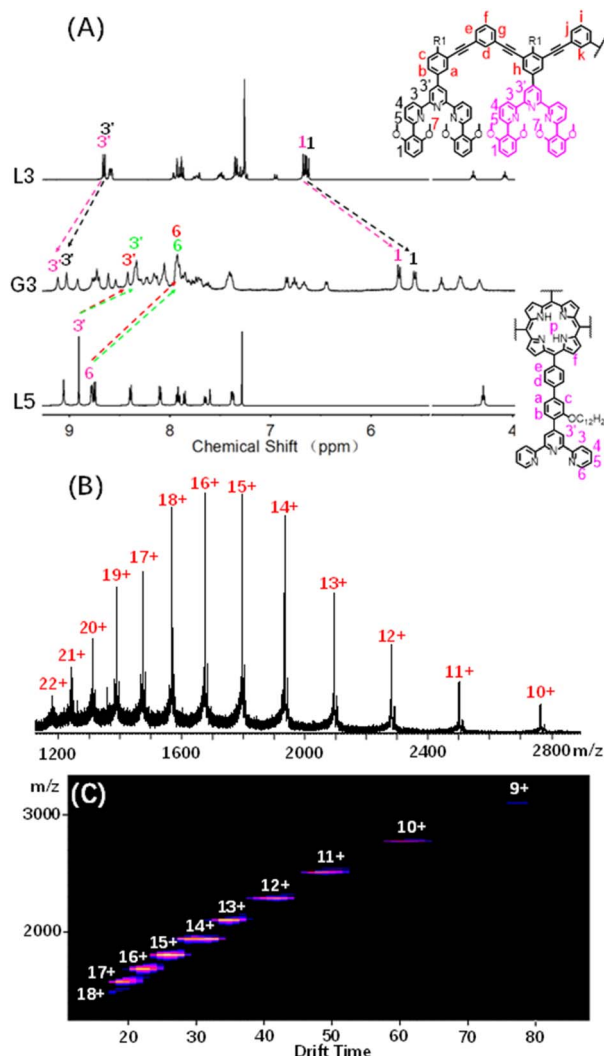


Fig. 4 (A) <sup>1</sup>H NMR spectra (500 MHz, 298 K) of G3 in CD<sub>3</sub>CN and L3 and L5 in CDCl<sub>3</sub>; (B) ESI-MS spectra and (C) 2D ESI-TWIM-MS plots of G3.

MS. The <sup>1</sup>H NMR spectrum showed that the H<sup>p</sup> signals can be fitted to three sets, respectively corresponding to G2, C<sub>60</sub>@G2 and (C<sub>60</sub>)<sub>2</sub>@G2, and the integration ratio of G2, C<sub>60</sub>@G2 and (C<sub>60</sub>)<sub>2</sub>@G2 was determined to be 5:9:4, manifesting that C<sub>60</sub>@G2 was the dominant product (Fig. 6C and S99<sup>†</sup>). Meanwhile, compared with G2, the <sup>13</sup>C NMR of (C<sub>60</sub>)<sub>n</sub>@G2 displayed a new broad single peak around 140.3 ppm composed of two slightly different signals belonging to C<sub>60</sub>, indicating that C<sub>60</sub> was successfully wrapped into the cavity because C<sub>60</sub> was originally nearly insoluble in acetonitrile (Fig. S100<sup>†</sup>). Moreover, as shown in Fig. 6A, the ESI-MS spectra in both CH<sub>3</sub>CN and DMF clearly showed three sets of consecutive peaks assigned to G2, C<sub>60</sub>@G2 and (C<sub>60</sub>)<sub>2</sub>@G2, respectively. And the content distribution of component G2, C<sub>60</sub>@G2 and (C<sub>60</sub>)<sub>2</sub>@G2 was further supported by the ESI-MS spectra (Fig. 6A and S102–S104<sup>†</sup>), which matched with the above-mentioned <sup>1</sup>H NMR analysis. To shed light on the recognition process, by using similar methods to C<sub>60</sub>@G1, the binding constants of C<sub>60</sub>@G2 and (C<sub>60</sub>)<sub>2</sub>@G2

were determined by UV titration as follows:  $K_1 = (3.06 \pm 0.5) \times 10^4 \text{ M}^{-1}$  and  $K_2 = (1.99 \pm 0.5) \times 10^4 \text{ M}^{-1}$  (Fig. S124 and S125<sup>†</sup>). Meanwhile, the kinetic process of G2 wrapping C<sub>60</sub> was monitored through time-dependent <sup>1</sup>H NMR experiments at 353 K. These <sup>1</sup>H NMR spectra showed that it took 18 h to achieve dynamic equilibrium of the (C<sub>60</sub>)<sub>n</sub>@G2 system (Fig. S101<sup>†</sup>), whereas just 13 h were required for C<sub>60</sub>@G1. Combining thermodynamics with kinetic data analysis, especially the cooperativity parameter ( $\alpha = 0.65 < 1$ ) in the process of G2 host–guest recognition (Fig. S125<sup>†</sup>),<sup>60</sup> we rationally proposed that the encapsulation of two guest molecules is a negative cooperation process,<sup>61</sup> namely one C<sub>60</sub> molecule entering the host cavity relatively increases the difficulty of accommodating the other one. To further prove this hypothesis, the total energy of states G2, C<sub>60</sub>, C<sub>60</sub>@G2 and (C<sub>60</sub>)<sub>2</sub>@G2 were also calculated using the semiempirical quantum mechanical GFN1-xTB method, and the corresponding binding energy ( $\Delta E$ ) for sequentially wrapping two C<sub>60</sub> was calculated to be  $-37.27 \text{ kcal mol}^{-1}$  (G2 + C<sub>60</sub> → C<sub>60</sub>@G2) and  $-15.56 \text{ kcal mol}^{-1}$  (C<sub>60</sub>@G2 + C<sub>60</sub> → (C<sub>60</sub>)<sub>2</sub>@G2) (Fig. 7A and S128<sup>†</sup>). Compared with the binding energy of C<sub>60</sub>@G1 ( $-23.47 \text{ kcal mol}^{-1}$ ) (Fig. S127<sup>†</sup>), G2 revealed stronger binding affinities to the first C<sub>60</sub>, whereas the binding energy of further encircling the second one to form (C<sub>60</sub>)<sub>2</sub>@G2 remained relatively lower, supporting that negative cooperation encapsulation behavior of two guest molecules.

Moving to (C<sub>60</sub>)<sub>n</sub>@G3 and (C<sub>60</sub>)<sub>n</sub>@G4, in spite of overly complex resonance signals which cannot be specifically assigned due to the possible presence of multiple adducts for (C<sub>60</sub>)<sub>n</sub>@G3 and (C<sub>60</sub>)<sub>n</sub>@G4, respectively (Fig. S126<sup>†</sup>), the fact that G3/G4 packaged multiple C<sub>60</sub> molecules can be supported by the multiple shifts of H<sup>p</sup> in <sup>1</sup>H NMR spectra in comparison to empty capsules G3/G4 (Fig. 6E, G, S106 and S112<sup>†</sup>). The asymmetric broad peaks belonging to C<sub>60</sub> in their <sup>13</sup>C NMR spectra further supported the encapsulation of multiple C<sub>60</sub> by G3 and G4 (Fig. S107 and S113<sup>†</sup>). Convincingly, the ESI-MS spectra clearly revealed the composition of multiple components for (C<sub>60</sub>)<sub>n</sub>@G3 and (C<sub>60</sub>)<sub>n</sub>@G4, in which (C<sub>60</sub>)<sub>n</sub>@G3 mixtures contained the main component (C<sub>60</sub>)<sub>2</sub>@G3 in addition to a small portion of C<sub>60</sub>@G3 and (C<sub>60</sub>)<sub>3</sub>@G3 (Fig. 6D, S109 and S110<sup>†</sup>), and (C<sub>60</sub>)<sub>n</sub>@G4 mixtures consisted of consecutive three sets of signal peaks belonging to (C<sub>60</sub>)<sub>2</sub>@G4, (C<sub>60</sub>)<sub>3</sub>@G4, and (C<sub>60</sub>)<sub>4</sub>@G4, respectively, with (C<sub>60</sub>)<sub>3</sub>@G4 being the main component (Fig. 6F, S115 and S116<sup>†</sup>). Monitoring of the dynamic process of G3/G4 wrapping C<sub>60</sub> at 353 K showed that G3/G4 wrapping C<sub>60</sub> to reach dynamic equilibrium needed nearly 20 hours (Fig. S108 and S114<sup>†</sup>), manifesting the slower multiple binding process. Finally, the total energy of various possible products for (C<sub>60</sub>)<sub>n</sub>@G3 and (C<sub>60</sub>)<sub>n</sub>@G4 was also calculated (Fig. S129 and S130<sup>†</sup>). Based on the tendency of each step to generate the corresponding host–guest complexes with the lowest energy, the proposed processes of G3 and G4 wrapping multiple C<sub>60</sub> and these corresponding binding energies ( $\Delta E$ ) were given (Fig. 7B and S131<sup>†</sup>). In the process of sequentially encapsulating C<sub>60</sub>, the binding energy revealed a downward trend and was the smallest for the last one which entered the cavities to form (C<sub>60</sub>)<sub>3</sub>@G3 and (C<sub>60</sub>)<sub>4</sub>@G4, which was calculated to be  $\Delta E_3 = -24.41 \text{ kcal mol}^{-1}$  and  $\Delta E_4 = -14.24 \text{ kcal}$

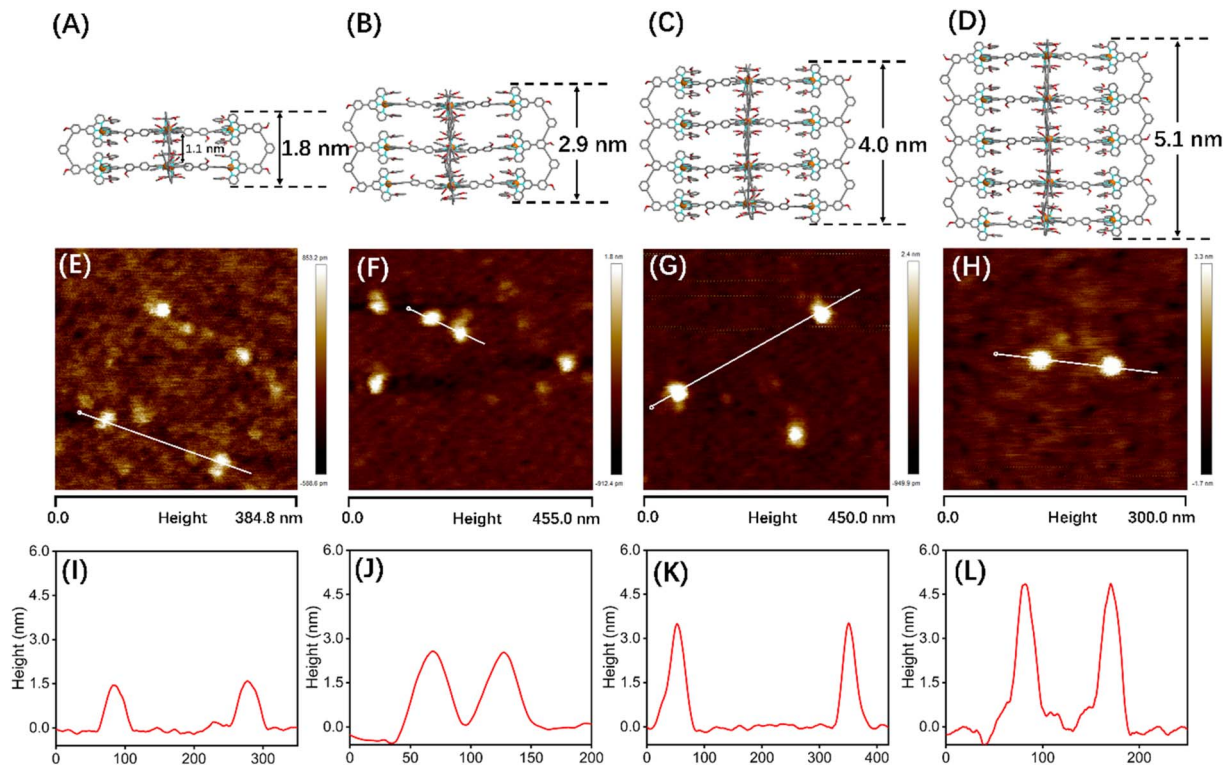


Fig. 5 Structures from Materials Studio-Forcite-Geometry Optimization (the saturated fatty chain in G2–G4 was simplified to the methoxy group), AFM images and height mapping of the selected single molecule: (A), (E) and (I) for G1, (B), (F) and (J) for G2, (C), (G) and (K) for G3, and (D), (H) and (L) for G4.

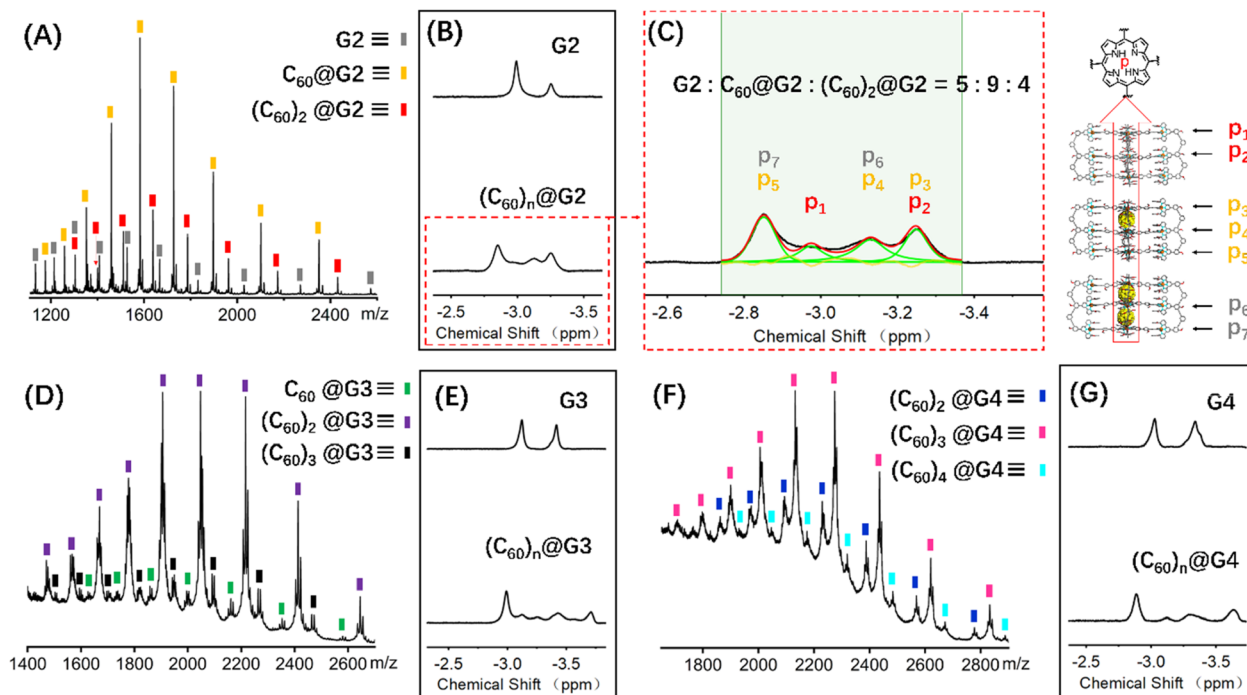


Fig. 6 ESI-MS spectra of the (A)  $(\text{C}_{60})_n\text{@G2}$ , (D)  $(\text{C}_{60})_n\text{@G3}$  and (F)  $(\text{C}_{60})_n\text{@G4}$ ,  $^1\text{H}$  NMR spectra (600 MHz, 298 K) comparison diagram of the  $\text{H}^p$  for (B) G2 and  $(\text{C}_{60})_n\text{@G2}$ , (E) G3 and  $(\text{C}_{60})_n\text{@G3}$ , (G) G4 and  $(\text{C}_{60})_n\text{@G4}$ , (C) the  $^1\text{H}$  NMR spectra attribution of  $\text{H}^p$  for  $(\text{C}_{60})_n\text{@G2}$  and the proportion of G2,  $\text{C}_{60}\text{@G2}$  and  $(\text{C}_{60})_2\text{@G2}$ .



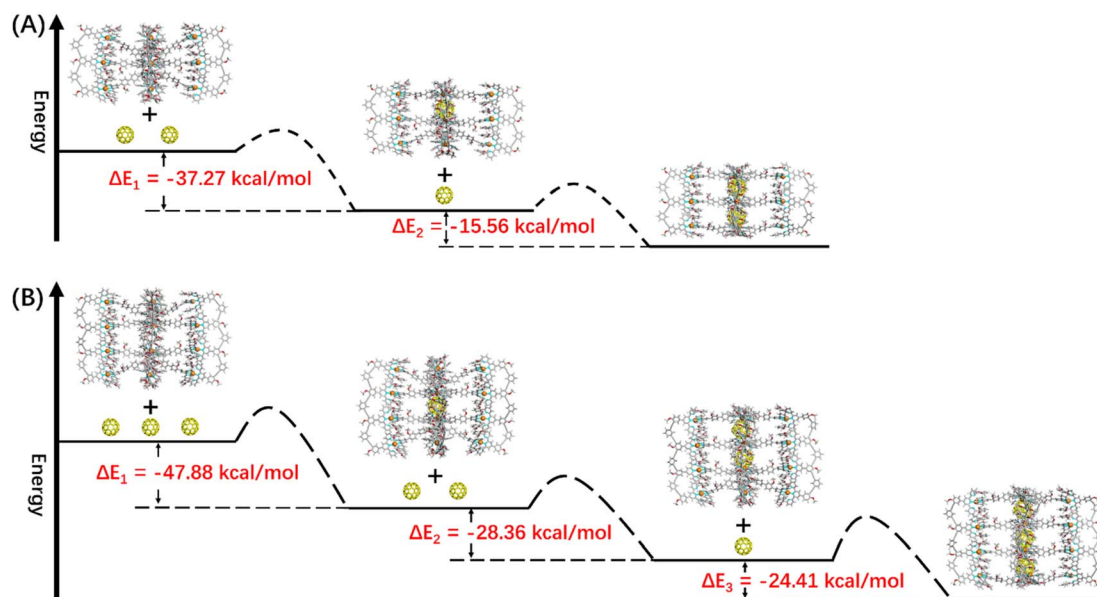


Fig. 7 The energy schematic diagram of the inferred main path and the corresponding binding energy for (A) G2 and (B) G3 wrapping  $C_{60}$ , respectively (the main path given by calculating the maximum energy difference).

$\text{mol}^{-1}$ , respectively (Fig. 7B and S131†). Such results were in accordance with the wrapping behavior of G2, verifying the negative cooperation performance in the process of multiple host recognition to guest  $C_{60}$  molecules for multideck capsules G2–G4. The negative cooperation behavior can be attributed to conformational adaptation, in which the entry of large-size guest molecules affects the molecular configuration, resulting in the volume decrease of remaining cavities, thereby increasing the energy of the entire system after subsequent guest molecule binding.<sup>42,62</sup> Similar collaborative behavior for the multi-guest recognition process in a single cavity was understandable because the electronic effects and spatial complementarity between multiple guests in a single-cavity host were strong.<sup>51,63–65</sup> However, the synergistic effect of capsules with multiple separate cavities is rarely reported, only observed in a few capsules with flexible cavities and strong conformational adaptation.<sup>66,67</sup> For herein reported capsules with rigid cavities, the negative cooperation behavior was possibly attributed to the large size of guest molecules and strong host–guest interactions.

In addition, the photosensitivity of capsule complexes with  $C_{60}$  ( $(C_{60})_n@Gn$ ) to generate singlet oxygen has been studied. The time-dependent UV-vis spectra under 405 nm irradiation were recorded and showed the gradually decreasing absorption intensity of DPHA, which can be ascribed to the formation of endoperoxide *via* singlet oxygen-mediated oxidation.<sup>68</sup> Such a result indicates that capsules loaded with  $C_{60}$  possess photosensitive properties (Fig. S133 and S134†). As the number of cavities increases, the ability of capsules to generate  $^1O_2$  increases, principally because of improved photosensitive performance *via* enhanced light capture as the number of porphyrin rings increases (Fig. S135†). These results provide a method for designing and synthesizing supramolecular structures with enhanced photosensitivity in the future.

## Conclusions

Overall, using the multi-component modular self-assembly strategy, we have designed and synthesized a series of complex layered metal–organic capsules G1–G4. These multideck structures possess different numbers of large and separate internal cavities formed by two parallel porphyrin planes and displayed strong recognition capability for large guest molecule  $C_{60}$  (the binding constant up to  $10^6$  M), convincingly supported by  $^1H$  NMR,  $^{13}C$  NMR, and ESI-MS spectroscopies, UV-vis titration and GFN1-xTB method calculation. Unprecedentedly, these multi-cavity capsules were exploited as multi-guest recognition systems and displayed intriguing binding performance up to four  $C_{60}$  at a time. Interestingly, the negative cooperation behavior was observed for the capsules G2–G4 in the process of binding multiple  $C_{60}$  molecules, which can be attributed to the scarce conformational adaptation of rigid capsules. This work provides a powerful strategy to construct complex metal–organic capsules with multiple cavities by multi-component coordination-driven self-assembly and establishes a novel platform for the study of host–guest interactions in multiple separate cavities, which lays a foundation for the construction of more complex host–guest systems in the future.

## Author contributions

K. L. conceived the project, synthesized the ligand molecules and completed the manuscript, which was supervised by D. L. and P. W. Characterization experiments including NMR, MS, AFM, and TEM were performed with the assistance of Z. L., M. C., J. W. and Z. J. All authors participated in the data analysis and discussions.



## Conflicts of interest

There is no conflict of interest to report.

## Acknowledgements

We acknowledge the support from the National Natural Science Foundation of China (22001047 for D. L. and 21971257 for P. W.). The authors gratefully acknowledge the Center for Advanced Research in CSU for the NMR measurements.

## Notes and references

- 1 K. Kinbara and T. Aida, *Chem. Rev.*, 2005, **105**, 1377–1400.
- 2 R. Chakrabarty, P. S. Mukherjee and P. J. Stang, *Chem. Rev.*, 2011, **111**, 6810–6918.
- 3 M. M. Smulders, I. A. Riddell, C. Browne and J. R. Nitschke, *Chem. Soc. Rev.*, 2013, **42**, 1728–1754.
- 4 X. Z. Li, C. B. Tian and Q. F. Sun, *Chem. Rev.*, 2022, **122**, 6374–6458.
- 5 Y. Zhu, W. Zheng, W. Wang and H. B. Yang, *Chem. Soc. Rev.*, 2021, **50**, 7395–7417.
- 6 H. Gotfredsen, J. R. Deng, J. M. Van Raden, M. Righetto, J. Hergenbahn, M. Clarke, A. Bellamy-Carter, J. Hart, J. O'Shea, T. D. W. Claridge, F. Duarte, A. Saywell, L. M. Herz and H. L. Anderson, *Nat. Chem.*, 2022, **14**, 1436–1442.
- 7 Z. Zhang, Y. Li, B. Song, Y. Zhang, X. Jiang, M. Wang, R. Tumbleson, C. Liu, P. Wang, X. Q. Hao, T. Rojas, A. T. Ngo, J. L. Sessler, G. R. Newkome, S. W. Hla and X. Li, *Nat. Chem.*, 2020, **12**, 468–474.
- 8 L. L. Yan and V. W. Yam, *J. Am. Chem. Soc.*, 2024, **146**, 609–616.
- 9 W. Xue, T. K. Ronson, Z. Lu and J. R. Nitschke, *J. Am. Chem. Soc.*, 2022, **144**, 6136–6142.
- 10 J. Koo, I. Kim, Y. Kim, D. Cho, I. C. Hwang, R. D. Mukhopadhyay and K. Kim, *Chem*, 2020, **6**, 3374–3384.
- 11 N. Takeda, K. Umemoto, K. Yamaguchi and M. Fujita, *Nature*, 1999, **398**, 794–796.
- 12 E. Benchimol, B. T. Nguyen, T. K. Ronson and J. R. Nitschke, *Chem. Soc. Rev.*, 2022, **51**, 5101–5135.
- 13 D. Fujita, Y. Ueda, S. Sato, N. Mizuno, T. Kumasaka and M. Fujita, *Nature*, 2016, **540**, 563–566.
- 14 S. Pullen, J. Tessarolo and G. H. Clever, *Chem. Sci.*, 2021, **12**, 7269–7293.
- 15 Z. Cui and G. X. Jin, *Nat. Synth.*, 2022, **1**, 635–640.
- 16 Z. Ashbridge, S. D. P. Fielden, D. A. Leigh, L. Pirvu, F. Schaufelberger and L. Zhang, *Chem. Soc. Rev.*, 2022, **51**, 7779–7809.
- 17 Y. Song, F. Schaufelberger, Z. Ashbridge, L. Pirvu, I. J. Vitorica-Yrezabal and D. A. Leigh, *Chem. Sci.*, 2020, **12**, 1826–1833.
- 18 R. Bai, Z. Zhang, W. Di, X. Yang, J. Zhao, H. Ouyang, G. Liu, X. Zhang, L. Cheng, Y. Cao, W. Yu and X. Yan, *J. Am. Chem. Soc.*, 2023, **145**, 9011–9020.
- 19 L. K. Moree, L. A. V. Faulkner and J. D. Crowley, *Chem. Soc. Rev.*, 2024, **53**, 25–46.
- 20 K. Wu, E. Benchimol, A. Baksi and G. H. Clever, *Nat. Chem.*, 2024, 584–591.
- 21 J. E. M. Lewis, A. Tarzia, A. J. P. White and K. E. Jelfs, *Chem. Sci.*, 2019, **11**, 677–683.
- 22 N. Pearce, M. Tarnowska, N. J. Andersen, A. Wahrhaftig-Lewis, B. S. Pilgrim and N. R. Champness, *Chem. Sci.*, 2022, **13**, 3915–3941.
- 23 Y. Li, H. Jiang, W. Zhang, X. Zhao, M. Sun, Y. Cui and Y. Liu, *J. Am. Chem. Soc.*, 2024, **146**, 3147–3159.
- 24 H. N. Zhang, H. J. Feng, Y. J. Lin and G. X. Jin, *J. Am. Chem. Soc.*, 2023, **145**, 4746–4756.
- 25 T. R. Schulte, J. J. Holstein, L. Schneider, A. Adam, G. Haberhauer and G. H. Clever, *Angew. Chem., Int. Ed.*, 2020, **59**, 22489–22493.
- 26 D. Liu, K. Li, M. Chen, T. Zhang, Z. Li, J. F. Yin, L. He, J. Wang, P. Yin, Y. T. Chan and P. Wang, *J. Am. Chem. Soc.*, 2021, **143**, 2537–2544.
- 27 E. Ubasart, O. Borodin, C. Fuertes-Espinosa, Y. Xu, C. Garcia-Simon, L. Gomez, J. Juanhuix, F. Gandara, I. Imaz, D. MasPOCH, M. von Delius and X. Ribas, *Nat. Chem.*, 2021, **13**, 420–427.
- 28 N. Ahmad, H. A. Younus, A. H. Chughtai and F. Verpoort, *Chem. Soc. Rev.*, 2015, **44**, 9–25.
- 29 D. Zhang, T. K. Ronson, Y. Q. Zou and J. R. Nitschke, *Nat. Rev. Chem.*, 2021, **5**, 168–182.
- 30 R. Saha, B. Mondal and P. S. Mukherjee, *Chem. Rev.*, 2022, **122**, 12244–12307.
- 31 T. K. Piskorz, V. Marti-Centelles, R. L. Spicer, F. Duarte and P. J. Lusby, *Chem. Sci.*, 2023, **14**, 11300–11331.
- 32 Y. Hou, Z. Zhang, S. Lu, J. Yuan, Q. Zhu, W. P. Chen, S. Ling, X. Li, Y. Z. Zheng, K. Zhu and M. Zhang, *J. Am. Chem. Soc.*, 2020, **142**, 18763–18768.
- 33 S. Lee, H. Jeong, D. Nam, M. S. Lah and W. Choe, *Chem. Soc. Rev.*, 2021, **50**, 528–555.
- 34 T. R. Cook and P. J. Stang, *Chem. Rev.*, 2015, **115**, 7001–7045.
- 35 R. A. S. Vasdev, D. Preston and J. D. Crowley, *Chem.-Asian J.*, 2017, **12**, 2513–2523.
- 36 F. J. Rizzuto, L. K. von Krbek and J. R. Nitschke, *Nat. Rev. Chem.*, 2019, **3**, 204–222.
- 37 R. Zhu, I. Regeni, J. J. Holstein, B. Dittrich, M. Simon, S. Prevost, M. Gradzielski and G. H. Clever, *Angew. Chem., Int. Ed.*, 2018, **57**, 13652–13656.
- 38 Y. Yamauchi, M. Yoshizawa and M. Fujita, *J. Am. Chem. Soc.*, 2008, **130**, 5832–5833.
- 39 W. M. Bloch, J. J. Holstein, B. Dittrich, W. Hiller and G. H. Clever, *Angew. Chem., Int. Ed.*, 2018, **57**, 5534–5538.
- 40 J. E. M. Lewis, *Angew. Chem., Int. Ed.*, 2022, **61**, e202212392.
- 41 L. S. Lisboa, D. Preston, C. J. McAdam, L. J. Wright, C. G. Hartinger and J. D. Crowley, *Angew. Chem., Int. Ed.*, 2022, **61**, e202201700.
- 42 K. Yazaki, M. Akita, S. Prusty, D. K. Chand, T. Kikuchi, H. Sato and M. Yoshizawa, *Nat. Commun.*, 2017, **8**, 15914.
- 43 D. Preston, J. E. Lewis and J. D. Crowley, *J. Am. Chem. Soc.*, 2017, **139**, 2379–2386.
- 44 M. D. Johnstone, E. K. Schwarze, G. H. Clever and F. M. Pfeffer, *Chem.-Eur. J.*, 2015, **21**, 3948–3955.





- 45 S. Bandi, A. K. Pal, G. S. Hanan and D. K. Chand, *Chem.–Eur. J.*, 2014, **20**, 13122–13126.
- 46 T. Yamaguchi, N. Ishii, K. Tashiro and T. Aida, *J. Am. Chem. Soc.*, 2003, **125**, 13934–13935.
- 47 J. D. Crowley, A. J. Goshe and B. Bosnich, *Chem. Commun.*, 2003, 2824–2825, DOI: [10.1039/b307385h](https://doi.org/10.1039/b307385h).
- 48 S. Y. Wang, J. Y. Huang, Y. P. Liang, Y. J. He, Y. S. Chen, Y. Y. Zhan, S. Hiraoka, Y. H. Liu, S. M. Peng and Y. T. Chan, *Chem.–Eur. J.*, 2018, **24**, 9274–9284.
- 49 W. Meng, B. Breiner, K. Rissanen, J. D. Thoburn, J. K. Clegg and J. R. Nitschke, *Angew. Chem., Int. Ed.*, 2011, **50**, 3479–3483.
- 50 J. Song, N. Aratani, H. Shinokubo and A. Osuka, *J. Am. Chem. Soc.*, 2010, **132**, 16356–16357.
- 51 F. J. Rizzuto, D. M. Wood, T. K. Ronson and J. R. Nitschke, *J. Am. Chem. Soc.*, 2017, **139**, 11008–11011.
- 52 K. Tashiro and T. Aida, *Chem. Soc. Rev.*, 2007, **36**, 189–197.
- 53 D. Rothschild, W. P. Kopcha, A. Tran, J. Zhang and M. C. Lipke, *Chem. Sci.*, 2022, **13**, 5325–5332.
- 54 P. Thordarson, *Chem. Soc. Rev.*, 2011, **40**, 1305–1323.
- 55 C. Bannwarth, S. Ehlert and S. Grimme, *J. Chem. Theory Comput.*, 2019, **15**, 1652–1671.
- 56 T. Ichijo, S. Sato and M. Fujita, *J. Am. Chem. Soc.*, 2013, **135**, 6786–6789.
- 57 M. Radmacher, M. Fritz, H. G. Hansma and P. K. Hansma, *Science*, 1994, **265**, 1577–1579.
- 58 Y. Yamauchi, M. Yoshizawa and M. Fujita, *J. Am. Chem. Soc.*, 2008, **130**, 5832–5833.
- 59 H. Sato, K. Tashiro, H. Shinmori, A. Osuka, Y. Murata, K. Komatsu and T. Aida, *J. Am. Chem. Soc.*, 2005, **127**, 13086–13087.
- 60 C. A. Hunter and H. L. Anderson, *Angew. Chem., Int. Ed.*, 2009, **48**, 7488–7499.
- 61 H. Sato, K. Tashiro, H. Shinmori, A. Osuka, Y. Murata, K. Komatsu and T. Aida, *J. Am. Chem. Soc.*, 2005, **127**, 13086–13087.
- 62 S. Mirtschin, A. Slabon-Turski, R. Scopelliti, A. H. Velders and K. Severin, *J. Am. Chem. Soc.*, 2010, **130**, 14004–14005.
- 63 G. H. Clever, W. Kawamura, S. Tashiro, M. Shiro and M. Shionoya, *Angew. Chem., Int. Ed.*, 2012, **51**, 2606–2609.
- 64 K. Ono, M. Yoshizawa, T. Kato, K. Watanabe and M. Fujita, *Angew. Chem., Int. Ed.*, 2007, **46**, 1803–1806.
- 65 H. Sato, K. Tashiro, H. Shinmori, A. Osuka, Y. Murata, K. Komatsu and T. Aida, *J. Am. Chem. Soc.*, 2005, **127**, 13086–13087.
- 66 S. Löffler, A. Wuttke, B. Zhang, J. J. Holstein, R. A. Mata and G. H. Clever, *Chem. Commun.*, 2017, **53**, 11933–11936.
- 67 S. Löffler, J. Lubben, L. Krause, D. Stalke, B. Dittrich and G. H. Clever, *J. Am. Chem. Soc.*, 2015, **137**, 1060–1063.
- 68 K. Gao, Y. Cheng, Z. Zhang, X. Huo, C. Guo, W. Fu, J. Xu, G. L. Hou, X. Shang and M. Zhang, *Angew. Chem., Int. Ed.*, 2024, **63**, e202319488.

